ITEP Lattice

arXiv:1203.5699v3 [hep-lat] 20 Aug 2012

The ρ and A mesons in a strong abelian magnetic field in SU(2) lattice gauge theory.

E.V. Luschevskaya[1] and O.V. Larina[1]

[1]*ITEP, B. Cheremushkinskaya 25, Moscow, 117218 Russia*

(Dated: March 26, 2012)

We calculate the correlators of vector, axial and pseudoscalar currents in the background of a strong abelian magnetic field in a pure $SU(2)$ gauge theory with improved action. Using the maximal entropy method and fitting the correlators by a coshinus function we extract masses of ρ and a meson ground states in different spatial directions. We found that with the growth of the external magnetic field the ρ meson mass along the magnetic field ρ_{33} decreases, while the masses of the components perpendicular to the magnetic field, ρ_{22} and ρ_{11} slowly increase. The axial meson mass along the magnetic field also diminishes with the value of the field. However in the perpendicular directions to the magnetic field the mass components a_{11} and a_{22} do not change up to magnetic field strength ~ 1 GeV and stay equal each other within the error bars.

PACS numbers: 11.30.Rd; 12.38.Gc; 13.40.-f

I. INTRODUCTION

Quantum Chromodymanics in the background of an external magnetic field is a rich realm for explorations as it presents a huge interest for physicists because of many reasons. At first the strong magnetic fields can be related to the formation of the early Universe. It is not clear whether these fields were fundamental or occur as a result of a mutual motion of charged particles at that era. It is suggested, that the magnetic fields ~ 2 GeV existed in the Early Universe during the electroweak phase transition [1]. It is known that there are objects in the cosmic space, called magnetars or neutron stars, having the magnetic field in their cores of the order ~ 1 MeV.

Many amazing effects were discovered experimentally and approved theoretically in the recent time. Experiments by the STAR collaboration at RHIC in Au-Au collisions showed that the chiral magnetic effect takes place in the noncentral heavy-ion collisions [2–4]. This effect was confirmed in ALICE experiment at LHC. The strenth of the magnetic field can reach $15 m_\pi^2 \sim 290\, MeV^2$ [5], that is of the order of hadronic scale. The magnetic field appears because of the mutual motion of the ions (it is known that a moving charged particle creates an electric and magnetic field around itself) and creates an asymmetry of charged particles emitted. The essence of this effect is an appearance of a charged asymmetry of charged particles, emitted from the different sides of the reaction plane. So, it occurs that such a strong magnetic field can be created in the Earth laboratories and it is possible to explore the quark - hadronic matter in such extreme conditions, thus making this system very interesting.

A strong enough magnetic field can lead to the modification of the QCD phase diagram. Phenomenological calculations point out that the temperature T_c of the transition from the confinement phase to the deconfinement one increases with the value of B and the transition becomes of the first order [6]. An increase of T_c is also predicted by models of Nambu-Jona-Lasinio type: NJL, EPNJL, PNJL [7] and PNJL$_8$ [8], Gross-Neveu model [9, 10]. The first prediction from lattice simulations for two flavour QCD about the behavior of the deconfining temperature and the chiral symmetry restoration with increasing of the magnetic field was made in [11]. Contrary to this result the lattice simulations with $N_f = 2{+}1$ flavours [12] shows the decreasing of T_c with magnetic field. However, the chiral perturbation theory predicts the opposite effect of decreasing the transition temperature with the magnetic field [13].

The same have also been studied a few years earlier, but for the case of a chromomagnetic (instead of magnetic) field, in [14–16].

The external magnetic fields lead to the enhancement of the chiral symmentry breaking in the background of the field [17–21]. The analytical calculations [22–24] predict a linear increase of chiral condensate with the magnetic field in the leading order. Lattice simulations show that the chiral condensate depends on the strength of the applied field as a power function with exponent $n = 1.6 \pm 0.2$ [25]. AdS/CFT approach shows the quadratic behaviour [26].

In [27] was provided the first numerical study of magnetic catalysis in QCD with dynamical fermions.

Recently it was obtained from the Nambu-Jona-Lasinio model that in strong magnetic field the vacuum becomes a superconductor [28]. The transition to the superconducting state occurs at the critical value of magnetic field equal to $B_c = m_\rho^2/e \simeq 10^{16}$ Tesla. The superconductivity is realized along the axis of the magnetic field only, and is accompanied by the condensation of ρ mesons. Further investigations in this direction have been done in lattice investigations and [29, 30] and point out at the presence of a superconducting phase at strong magnetic fields. In our present work we explore the behaviour of the ρ and a meson ground states in the abelian strong magnetic field. We observed a deacrese of the meson masses in the direction of the magnetic field. We work in SU(2) gluodynamics because we are interested in qualitative predictions for the beginning. This model contains the main properties of the full QCD theory and easy for numerical simulations.

The paper is organized in the following way. In Section II we describe the technical and numerical setup of our simulations. We discuss measured observables in Section III. Section IV is devoted to the methods which we use. The results of our calculations are presented in Section VI. Our results are compared with the previous ones.

II. TECHNICAL DETAILS AND NUMERICAL SETUP

For the generation of $SU(2)$ quenched configurations we use the tadpole improved Symanzik action

$$S = \beta_{imp} \sum_{pl} S_{pl} - \frac{\beta_{imp}}{20u_0^2} \sum_{rt} S_{rt}, \tag{1}$$

where $S_{pl,rt} = (1/2)\mathrm{Tr}\,(1 - U_{pl,rt})$ is the plaquette (denoted by pl) or $1{\times}2$ rectangular loop term (rt), $u_0 = (W_{1\times1})^{1/4} = \langle(1/2)\mathrm{Tr}\,U_{pl}\rangle^{1/4}$ is the input tadpole factor, computed at zero temperature [31]. This action suppresses the ultraviolet dislocations, leading to unphysical near-zero modes of the Wilson-Dirac operator.

For the calculation of the fermion spectrum we use the chiral invariant massless Neuberger operator [32]. It is a nontrivial construction, allowing to preserve the chiral symmetry on the lattice and exploit the perfect chiral properties of the Dirac eigenmodes.

$$D_{ov} = \frac{\rho}{a}\left(1 + D_W/\sqrt{D_W^\dagger D_W}\right), \tag{2}$$

where $D_W = M - \rho/a$ is the Wilson-Dirac operator with a negative mass term ρ/a, a is the lattice spacing, M is the Wilson hopping term with $r = 1$. Anti-periodic boundary conditions in time and periodic ones in spatial directions are imposed to the fermionic fields in the overlap Dirac operator. Using the minmax polynomial approximation, we calculate the sign function.

$$D_W/\sqrt{D^\dagger D_W} = \gamma_5 \mathrm{sign}\,(H_W), \tag{3}$$

where $H_W = \gamma_5 D_W$ is the hermitian Wilson-Dirac operator. We treated the 30-50 lowest Wilson-Dirac eigenmodes separately for the calculation of the sign function.

In the continuum the analog of this operator is $D = \gamma^\mu(\partial_\mu - iA_\mu)$, satisfying the Dirac equation

$$D\psi_k = i\lambda_k\psi_k. \tag{4}$$

Here A_μ is the gauge field, ψ_k is the eigenmode and λ_k is the corresponding eigenvalue. The overlap operator D_{ov} measures the spectrum of the eigenmodes and eigenvalues of the probe quark, which we put into the gauge background $\langle A_\mu\rangle$ of gluodynamics. The eigenmodes of the Dirac operator allow to construct operators and correlators, which we talk about in Section 3.

We include the external uniform magnetic abelian field in the simulations. The abelian field interacts only with fermionic fields, so we introduce it only into Dirac operator without any modification of the gauge action by the following exchange

$$A_{\mu\,ij} \to A_{\mu\,ij} + A_\mu^B \delta_{ij}, \tag{5}$$

$$A_\mu^B(x) = \frac{B}{2}(x_1\delta_{\mu,2} - x_2\delta_{\mu,1}). \tag{6}$$

Expression (5) is valid in an infinite space, therefore to combine it with the periodic boundary conditions on the lattice we have to introduce an additional x-dependent twist for fermions, as expalained in [33].

The magnetic field in our calculations is directed along the third axes, it's value is discretized,

$$qB = \frac{2\pi k}{(aL)^2}, \quad k \in \mathbb{Z}, \tag{7}$$

because the lattice represents a finite 4 dimentional box, we have the only one type of quarks and take its charge $q = -1/3\,e$, which corresponds to the d-quark. The quantization condition posses a restriction to the minimal value of the magnetic field considering on the lattice. For example on the 16^4 with spacing $a = 0.0998$ fm the minimal value $\sqrt{eB} = 535.64$ MeV For inversion, we use a Gaussian source with radius $r = 1.0$ in lattice units in both spatial and time directions and a point sink (that is, quark position is smeared over a Gaussian profile).

We performed the calculations at 14^4 and 16^6 lattices for different lattice cutoff, $a = 0.0681,\ 0.0998$ and 0.138348 fm in order to control the effects of finite lattice spacing and volume. We used 300 configurations for the 14^4 lattice with $a = 0.138348$ fm. However for the other lattices the statistics is small $\sim 100 - 150$ configurations and we are increasing it now to make the extrapolations later. We also perform the simulations at different quark bare masses from $m_q a = 0.01$ till 0.5 in lattice units. For quark masses larger than $0.1 - 0.2$ the procedure works well and we get the good results with the reasonable errors.

III. OBSERVABLES

We calculate on the lattice the observables of the type

$$\langle\psi^\dagger(x)O_1\psi(x)\psi^\dagger(y)O_2\psi(y)\rangle_A, \tag{8}$$

where $O_1, O_2 = \gamma_5,\ \gamma_5\gamma_\mu,\ \gamma_\mu$. In the Euclidean space $\psi^\dagger = \bar\psi$ [34]. These current-current correlators in the meson channel can be represented in terms of Dirac propagators in the background of the gluonic fields and abelian constant magnetic field. In the continuum field theory (8) can be written in the following way

$$\int DA_\mu e^{-S_{YM}[A_\mu]}\left[\mathrm{Tr}\left(\frac{1}{D+m}O_1\right)\mathrm{Tr}\left(\frac{1}{D+m}O_2\right)\right] - \tag{9}$$

$$\int DA_\mu e^{-S_{YM}}[A_\mu]\left[\mathrm{Tr}\left(\frac{1}{D+m}O_1\frac{1}{D+m}O_2\right)\right].$$

The first term in the difference is the disconnected part, while the second one is connected . The disconnected part is very intricate for the calculations and has big errors. We check that the disconnected contribution is significantly smaller than the connected one and can be excepted from the consideration. So, we calculate only the connected part of the correlator (9).

We calculate the Dirac propagator on the lattice by inverting the massive Dirac operator $1/(D+m)$ in the subspace of M $(30, 50$ in our case) eigenvectors with the λ_k lowest eigenvalues. It has the form

$$\frac{1}{D+m}(x,y)=\sum_{k<M}\frac{\psi_k(x)\psi_k^\dagger(y)}{i\lambda_k+m}. \qquad (10)$$

Taking into account (10) one can reformulate (9) on the lattice

$$\langle\bar\psi O_1\psi\bar\psi O_2\psi\rangle_A \qquad (11)$$

$$=\sum_{k,p<M}\frac{\langle k|O_1|k\rangle\langle p|O_2|p\rangle-\langle p|O_1|k\rangle\langle k|O_2|p\rangle}{(i\lambda_k+m)(i\lambda_p+m)}$$

The first term in 9 is not essential as we have said above. The magnetic and gluonic fields are incorporated into the consideration in the way described above.

The mass of neutral ρ-meson was extracted from the vector correlator of the vector currents $\langle j_\mu^V(x)j_\nu^V(y)\rangle_A$, where $j_\mu^V(x)=\psi^\dagger(x)\gamma_\mu\psi(x)$, the mass of the neutral axial meson - from the correlator of axial currents $\langle j_\mu^A(x)j_\nu^A(y)\rangle_A$, where $j_\mu^A(x)=\psi^\dagger(x)\gamma_\mu\gamma_5\psi(x)$ is the axial current. The correlator $\langle j^{PS}(x)j^{PS}(y)\rangle_A$ corresponds to π-meson, here $j^{PS}=\psi^\dagger(x)\gamma_5\psi(x)$ is pseudoscalar current.

IV. METHODS

We use two methods for the calculations of the masses. In the first method we consider the imaginary parts of the corresponding correlators and project the sink operator to zero spatial momentum. We get

$$\langle\psi^\dagger(\vec 0,n_t)O_1\psi(\vec 0,n_t)\psi^\dagger(\vec 0,0)O_2\psi(\vec 0,0)\rangle_A= \qquad (12)$$

$$\sum_k\langle 0|O_1|k\rangle\langle k|O_2^\dagger|0\rangle e^{-n_tE_k}.$$

For a finite lattice the values of E_k are discrete. For the single particle intermediate states the mass $m_k=E_k$, i.e. coincides with the low-lying energy value. We are interested in the ground state energyes of the mesons and its dependence from the magnetic field.

The first term $\langle 0|O_1|k\rangle\langle k|O_2^\dagger|0\rangle e^{-n_tE_0}$ in (12) gives the main contribution to the sum for the large values of lattice time slice n_t. For this reason we fit the corresponding imaginary part of the correlators in the minimum by the coshinus function of the form $C(n_t)=A\cosh(m_{eff}(n_t-N_T/2))$ on the interval $4<n_t<N_T-4$ for different n_t and making averaging (fitting with different n_t reduces the errors), Extract the mass m_{eff} from the fit, N_T is the lattice temporal extention and get sufficiently good fits for the correlators within the range of error bars.

The second method which we use is the Maximal Entropy Method (MEM) [35]. The imaginary-time Euclidean correlator $G(\tau,\vec p)=\int d^3\,x\langle O(\tau,\vec x)O^\dagger(0,\vec 0)\rangle e^{-i\vec p\vec x}$ is related to the spectral function $\rho(\omega,\vec p)$ according to

$$G(\tau,\vec p)=\int_0^\infty\frac{d\omega}{2\pi}K(\tau,\omega)\rho(\omega,\vec p). \qquad (13)$$

In general $\rho(\omega,\vec p)$ carries the all properties of mesons and hadrons. We consider $\vec p=0$ and drope the $\vec p$ dependence in the following. The peak in the spectral function corresponds to the energy of the ground state. The kernel in (13) is given by

$$K(\tau,\omega)=\frac{\cosh[\omega(\tau-1/2T)]}{\sinh(\omega/2T)}, \qquad (14)$$

where T is the temperature, τ is the euclidean time, ω is the frequency. To extract the spectral function from (13) one can try to make an inversion.

On the lattice this problem is ill-defined, because we calculate the correlator $G(\tau)$ numerically at the discrete set of points $\tau_i=\tau_{min}+(i-1)a$, where a is the lattice spacing, $i=1,...N_\tau$, $N_\tau=1/(aT)$ is typically of the order of $O(10)$. Then we approximate the integral by a discrete sum at the points $\omega_n=n\triangle\omega$, $n=1,...,N_\omega$ and N_ω is usually $\sim O(10^3)$. We cutoff the integral (13) at some ω_{max}. All the same the inversion becomes impossible. But the ideas of Bayesian probability theory allow to overcome this difficulty.

The most probable spectral function $\rho(\omega)$ can be constructed if we find the maximum of the conditional probability $P[\rho|DH\alpha m]$, where D is the data,H is our hypothesis, α is a real and positive parameter, $m=m(\omega)$ is the default model which we use. This procedure is equivalent to a maximization of the free energy $F=L-\alpha S$, where S is the Shannon entropy term, defined by the following way

$$S=\int_0^\infty d\omega\left[\rho(\omega)-m(\omega)-\rho(\omega)\ln\frac{\rho(\omega)}{m(\omega)}\right]. \qquad (15)$$

L is the standard likelihood function, the detailed explanation how to make a corresponding discretization on the lattice is given in [35]. The parameter α balances the relative importance of the data and the prior hypothesis. We take $\alpha\in[\alpha_{min},\alpha_{max}]$ and average the data over this interval. This interval was choosen in such way that the results vary slightly, for approximately 10%.

The kernel (14) contains divergence at $\omega = 0$ leading to unstable behaviour of the procedure at small energies. The Bryan's key idea was to redefine the kernel and spectral function

$$\bar{K}(\omega,\tau) = \frac{\omega}{2T} K(\omega,\tau), \qquad \bar{\rho}(\omega) = \frac{2T}{\omega}\rho(\omega) \tag{16}$$

so that $K(\omega,\tau)\rho(\omega) = \bar{K}(\omega,\tau)\bar{\rho}(\omega)$ and apply the SVD theorem to the modified discretized kernel $\bar{K}(\omega_n,\tau_i)$, see [36]. We use this modified algorithm to determine the spectral function in the form

$$\bar{\rho}(\omega) = \bar{m}(\omega) \exp \sum_{i=1}^{N} \bar{c}_i \bar{u}_i(\omega). \tag{17}$$

The column vectors u_i, $(i = 1, .., N)$ are normalized

$$\langle u_i | u_j \rangle \equiv \sum_{n=1}^{N_\omega} u_i(\omega_n) u_j(\omega_n) = \delta_{ij}, \tag{18}$$

c_i are the coefficients and we set $\bar{K}(0,\tau) = 1$.

Therefore to reconstruct the spectral function $\rho(\omega)$ we have to choose the default model $\bar{m}(\omega)$ in a correct way. The default model should describe correctly the high and low energy behaviour of the spectral function. Following the analysis of [37] we choose it in the form

$$\bar{m}(\omega) = m_a\omega + m_b, \quad m_a = \frac{G(N_\tau/2)}{T^2}, \quad m_b = a_H \frac{3}{8\pi^2}, \tag{19}$$

$a_H = 1$ for scalar and pseudoscalar channel, $a_H = 2$ for vector and axial vector channel [38]. We also try another default model (constant function, $\sim \omega^2$, vary the m_a and m_b), but the choice (19) gives the best convergence of MEM.

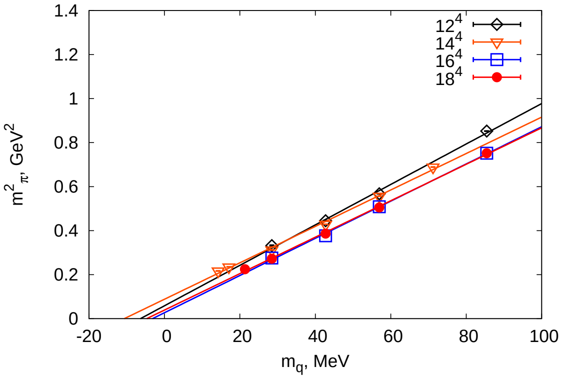

FIG. 1: The squared mass of the neutral π meson extracted from the $C^{PSPS}(n_t)$ versus the bare lattice quark mass for 14^4 lattice volume, lattice spacing 0.1383 fm, $\beta = 3.1000$ and different values of an external magnetic field.

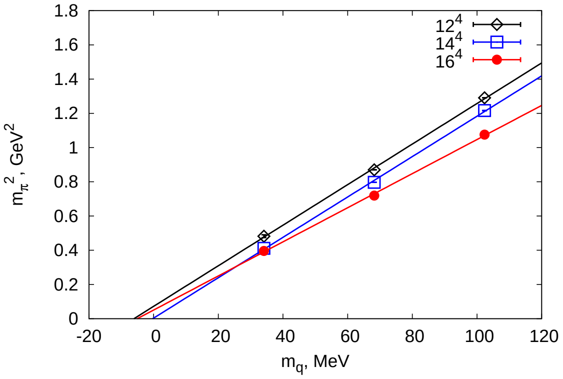

FIG. 2: The same that in Figure 1, but for the lattice spacing 0.1155 fm, $\beta = 3.2000$.

V. VECTOR MESON MASS AT $B = 0$

At this section we present the calculation of ρ meson mass in $SU(2)$ gluodynamics for zero magnetic field. We compare our results with the previous one to be sure that our method works correctly. We measure the correlator of pseudoscalar currents $C^{PSPS}(n_t) = \langle j^{PS}(\vec{0},n_t) j^{PS}(\vec{0},0)\rangle_A$, where $j^{PS}(\vec{0},n_t) = \bar{\psi}(\vec{0},n_t)\gamma_5\psi(\vec{0},n_t)$ and calculate the mass of the lowest energy state of the neutral π meson for different quark masses, volumes and lattice spacings, see Figure 1 and 2.

We get the linear dependence of the squared π meson mass from the bare quark mass. It is known that the Chiral Perturbation Theory predicts such linear dependence according to the relation

$$f_\pi^2 m_\pi^2 = m_q^{ren} \langle \bar{\psi}\psi \rangle, \tag{20}$$

where f_π is the pion decay constant, $\langle\bar{\psi}\psi\rangle$ is the chiral condensate, m_q^{ren} is the renormalized quark mass. In the limit of zero quark mass we get massless pions. On the lattice we work with a bare quark mass. We see from the Figures 1 and 2 that the corresponding lines are shifted with respect to the origin of the coordinates and the value of quark mass renormalization slightly varies for the different lattice volumes and spacings within $0 - 10$ MeV and its precise determination is impossible for small volumes.

The mass of neutral ρ meson is calculated from the correlator of vector currents $C^{VV}(n_t) = \langle j^V_\mu(\vec{0},n_t) j^V_\nu(\vec{0},0)\rangle_A$, where $j^V_\mu(\vec{0},n_t) = \bar{\psi}(\vec{0},n_t)\gamma_\mu\psi(\vec{0},n_t)$ from the coshinus fits Then we perform the extrapolation to the infinite physical volume. We ignore the difference in the value of quark mass renormalization for different lattice volumes for a given lattice spacing and just take the averaged value. Later we see that the ρ meson mass is not very sensitive to the quark mass renormalization, at least the shift in quark mass for $10 - 20$ MeV doesn't change m_ρ. The extrapolation of ρ meson mass to the infinite physical volume limit was performed for several values of quark mass and two lattice spacings 0.1383 fm and 0.1155 fm (Figures 4 and 4). The best fit gives the $1/V_{phys}$ volume dependence, $V_{phys} = (aL)^3$, the power functions of the physical volumes give the worse fits.

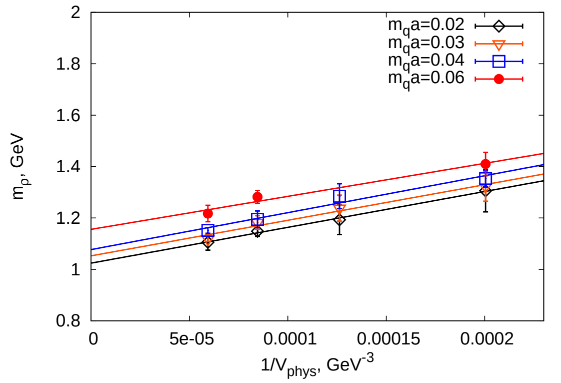

FIG. 3: The mass of the neutral ρ meson extracted from the $C^{VV}(n_t)$ for several bare quark masses, lattice volumes and lattice spacing 0.1383 fm, $\beta = 3.1000$. Magnetic field equals zero. Stars correspond to the extrapolated values of mass.

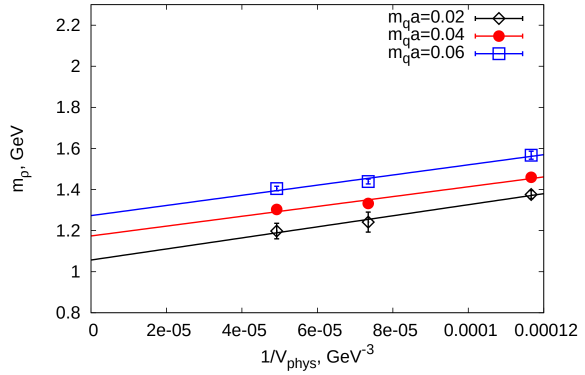

FIG. 4: The same that in Figure 3, but for the lattice spacing 0.1155 fm, $\beta = 3.2000$.

The second step is the quark mass extrapolation. The corresponding dependences are shown at Figure 5. We take the value of m_ρ meson mass at the physical value of quark mass 3 MeV. The corresponding pseudoscalar mass $m_\pi \simeq 150 - 250$ MeV (in depence on lattice parameters). The vector meson mass $m_\rho \simeq 932 \pm 12$ MeV for $a = 0.1338$ fm and 937 ± 12 MeV $a = 0.1155$ fm lattice, that is in agreement with the previous evaluations. The corresponding points are depicted by stars. The extrapolations were performed to the quark mass $m_q^{ph} = 3$ MeV, taking into account quark mass renormalization on the lattice. In our consideration the light quarks are degenerate.

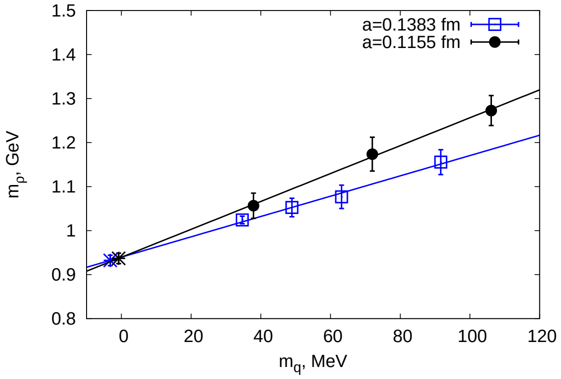

FIG. 5: The mass of ρ meson for the different quark masses and two lattice spacings. The extrapolated values of masses are depicted by stars and corresponds to the physical quark mass $m_q^{ph} = 3$ MeV.

VI. THE MASSES OF MESONS AT $B \neq 0$

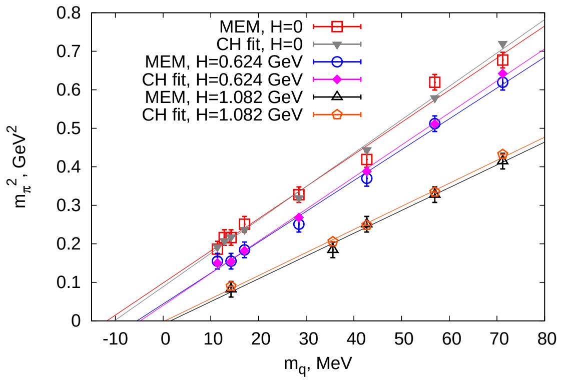

FIG. 6: The squared mass of the neutral π meson extracted from the $C^{PSPS}(n_t)$ versus the bare lattice quark mass for 14^4 lattice volume, lattice spacing 0.1383 fm, $\beta = 3.1000$ and different values of an external magnetic field.

At Figure 6 the squared pion mass is depicted for different bare quark mass and different values of magnetic fields $H = \sqrt{eB}$. The results obtained from the Maximal Entropy Method agree with the ones from the coshinus fitting. Both methods give the linear dependence, that is legitimate for the the Chiral Perturbation Theory, because this behaviour is in accordance with the relation

From the (20) dependence and Figure 6 we conclude that the quark mass on the lattice in the background of the gluon and abelian magnetic field have to be renormalized and this renormalization depends on the magnetic field value (because the line is shifted for different values of B with respect to the origin of coordinates).

We show the dependence of the π - meson mass from the value of the squared magnetic field, see Figure 7. It

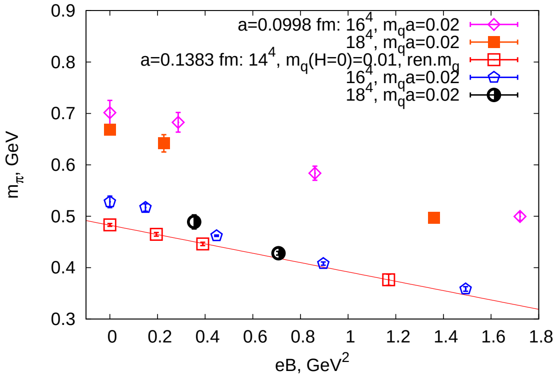

FIG. 7: The mass of the neutral π meson extracted from the $C^{PSPS}(n_t)$ versus the squared value of magnetic field for renormalized and nonrenormalized quark mass.

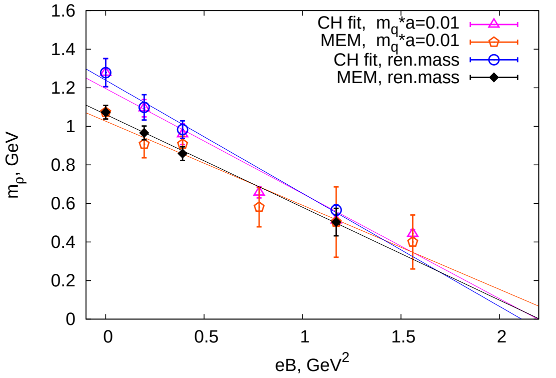

FIG. 8: The ρ_{33} meson mass component along the direction of B, extracted from the $C_{33}^{VV}(n_t)$, versus the squared value of the field for 14^4 lattice volume, lattice spacing 0.1383 fm, $\beta = 3.1000$ for renormalized quark mass and for the bare one $m_q a = 0.01$. The data are calculated by the MEM procedure and cosh-function fitting.

appears that the mass of π is very sensitive to the quark mass renormalization, doesn't depend on the lattice volume. For the magnetic fields less than 1 GeV we get the linear mass dependence from the magnetic field, the slope is negative, that is in accordance with the results of A.Smilga, obtained in chiral perturbation theory [24]. The value of the slope is smaller and differs from ChPT, because we explore the simpler $SU(2)$ gauge theory without dinamical quarks and only qualitative behaviour has sence.

The errors of MEM are very difficult to estimate, for the simplicity we take an ansamble of $O(10)$ results of MEM procedure and calculate an average and standard deviation for the best set of MEM parameters. Errors are calculated taking into account also the ω-discretization.

We calculate the components of the correlator of vector currents, the diagonal components are essentially nonzero, while the nondiagonal ones are zero within the error bars. The external magnetic field is directed along the third coordinate axes. The spatial diagonal components of the correlators perpendicular to the magnetic field are $C_{11}^{VV}(n_t) = \langle j_1^V(\vec{0}, n_t) j_1^V(\vec{0}, 0)\rangle_A$ and $C_{22}^{VV}(n_t) = \langle j_2^V(\vec{0}, n_t) j_2^V(\vec{0}, 0)\rangle_A$, where $j_1^V(\vec{0}, n_t) = \bar{\psi}(\vec{0}, 0)\gamma_1\psi(\vec{0}, n_t)$ and so on. The component along the direction of the magnetic field is $C_{33}^{VV}(n_t) = \langle j_3^V(\vec{0}, n_t) j_3^V(\vec{0}, 0)\rangle_A$. We fit the correlators by the coshinus function and also apply the MEM for the extracting the spectral functions for the each correlator. The position of a peak at $\omega \neq 0$ of a spectral function corresponds to the mass of the state in our case. The Euclidean time C_{00}^{VV} component is constant, in accordance with the conservation law of an electric charge, $\partial^\mu j_\mu^V = 0$. The C_{00}^{VV} componant gives just a peak at $\omega = 0$, we do not consider it here.

Let's denote the masses extracted from the correlators perpendicular to the magnetic field by ρ_{11} and ρ_{22} and the mass component along the field by ρ_{33}. Figure 8

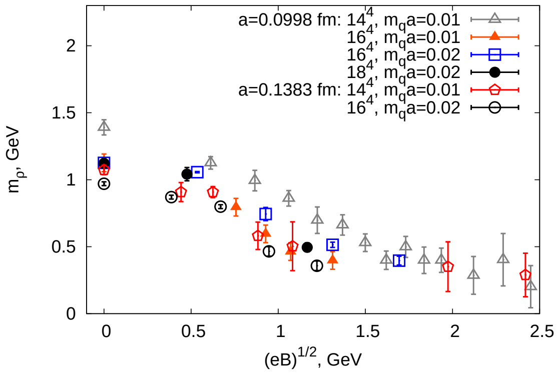

FIG. 9: The ρ_{33} mass along the direction of B, extracted from the $C_{33}^{VV}(n_t)$ correlator for 14^4 and 16^4 lattices and different lattice spacings, obtained from Maximal Entropy Method.

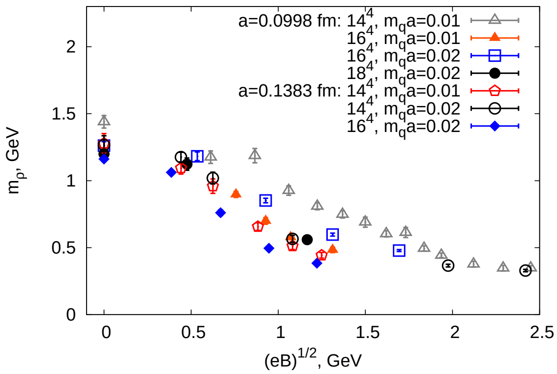

FIG. 10: The same that at Figure 9 but from the cosh-function fit of the correlators.

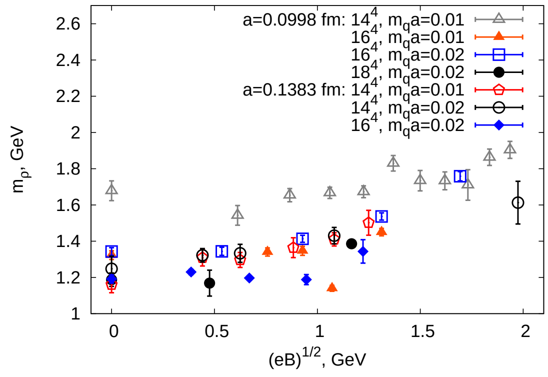

FIG. 11: The ρ_{11} meson mass extracted from the $C_{11}^{VV}(n_t)$ correlator perpendicular to the direction of B for 14^4 and 16^4 lattices and for different lattice spacings from coshinus function fit the correlators.

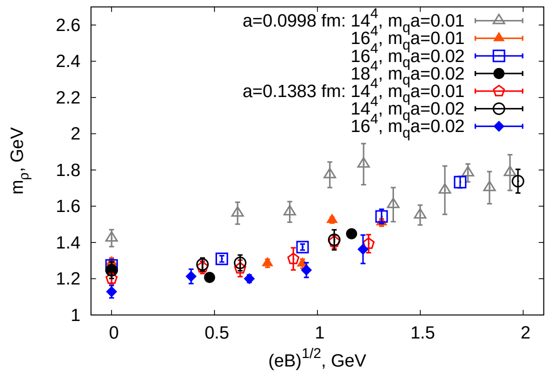

FIG. 12: The ρ_{22} meson mass extracted from the $C_{22}^{VV}(n_t)$ correlator for the same set of parameters and the method.

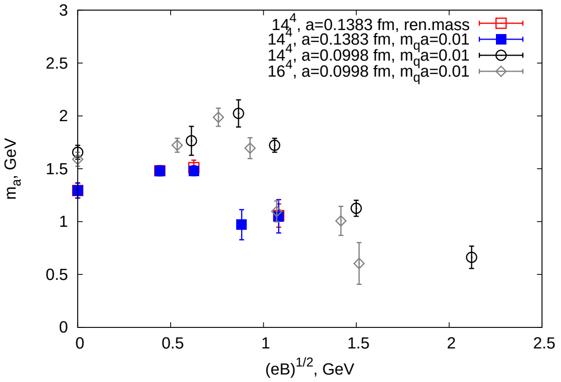

FIG. 13: The a_{33} mass, extracted from the $C_{33}^{AA}(n_t)$ correlator along the direction of eB for 14^4 and 16^4 lattices and for different lattice spacings by means of MEM procedure.

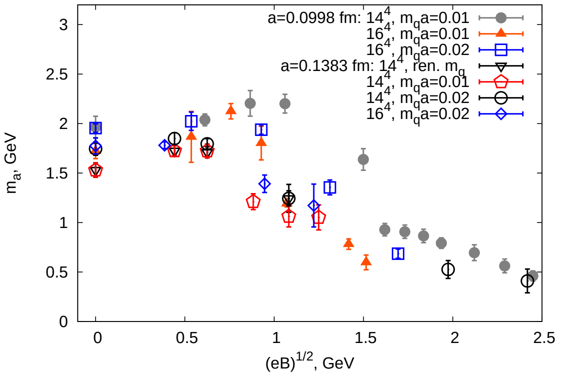

FIG. 14: The a_{33} mass, extracted from the $C_{33}^{AA}(n_t)$ correlator along the direction of B for 14^4 and 16^4 lattices and for different lattice spacings from MEM procedure.

shows that the mass of ρ_{33}, obtained from the $C_{33}^{VV}(n_t)$, along the direction of the magnetic field is insensitive to the renormalization.

We see that the ρ_{33} masses obtained with Maximum Entropy Procedure is a little bit lower that the masses extracted from the coshinus fit, it was to be expected because the MEM adjusts the correlators better than the coshinus fit does. Because the ρ mass doesn't depend on the renormalization we explore its behaviour for the bare quark mass $m_q a = 0.01$. The fit at Figure 8 is a linear function in eB for the fields till 1 GeV. It's slope is equal to $c \simeq -0.5$. In NJL approach [30] the neutral ρ meson doesn't depend on the magnetic field and the slope $c_1 = 1$, for the charged $\rho_\pm$ the slope $c_2 \sim -0.6$ for the interval $[0, 0.4]$ GeV.

At Figure 9 we depict the ρ_{33} mass, calculated from the $C_{33}^{VV}(n_t)$ correlator, but in another scale, versus $\sqrt{eB}$, and for the larger values of the magnetic field. The same dependence, but obtained with coshinus fit the correlators, is shown at Figure 10. We see that the ρ_{33} mass is decreasing with the growth of magnetic field and this takes place for the all lattices which we consider. However near the 1 GeV the squared behaviour in B changes to the asymptotic one. We need the bigger lattices and statistics to perform extrapolations and check this behaviour.

The ρ_{11} and ρ_{22} masses, obtained from the C_{11} and C_{22} correlators are shown at Figure 11 and 12. In contrast to ρ_{33}, obtained from C_{33}, ρ_{11} and ρ_{22} mass components increase with the field slowly. We observe the mass splitting because the external magnetic field create the anysotropy. In the absense of the magnetic field the masses ρ_{11}, ρ_{22} and ρ_{33}, extracted from the all correlators, coincide within the statistical errors.

We also calculate the axial correlator for the different lattice parameters and magnetic fields and extract the

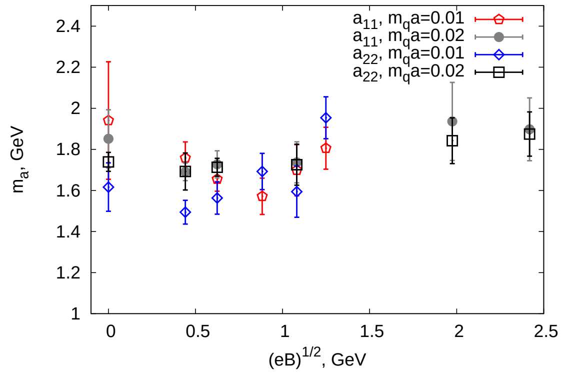

FIG. 15: The a_{ii}, $i = 1, 2$ masses, extracted from the $C_{ii}^{AA}(n_t)$ correlator perpendicular to the direction of B.

lowest energy state. The a_{33} extracted from the $C_{33}^{AA}(n_t)$ along the direction of the magnetic field is depicted at Figure 13 (MEM) and 14 (coshinus fit the correlators). We observe the decreasing of a_{33} mass component along the magnetic field. The peak around 1 GeV can be just a lattice artefact.

In the perpendicular direction to the magnetic field a_{11} and a_{22} masses do not reveal any dependence on the magnetic field till 1 GeV. We can see this from Figure 15. a_{ii}, $i = 1, 2, 3$ are also independent on the quark mass renormalization.

VII. LATTICE EXTRAPOLATIONS AT $B \neq 0$

On the lattice we work with discrete values of the external magnetic field. The value of magnetic field is determined according to 7 and as it follows from this formula depends on the lattice volume $(aL)^3$ and lattice spacing a. For this reason it's difficult to make lattice extrapolations to the continuum. At Figure 16 the dependences of the $m_{\rho_{33}}$ component (along the magnetic field) from the bare quark lattice mass are depicted to demostrate how we make a mass extrapolation. The third ρ mass component was shown here for the lattice volume 14^4, the magnetic field $H = 6$ in lattice units, but for different lattice spacings 0.0998, 0.1155 and 0.1383 fm. Cause the lattice spacings are different the values of magnetic field also differ. We fit the dependences by $m_\rho = a_0 + a_1 m_q + a_2 m_q^2$ function, which gives the best fit. We make a renormalization of lattice quark mass and after that extrapolate the mass of ρ meson to the point, where the physical quark mass is equal 3 MeV (marked by stars). As we mentioned above this value gives the mass of π meson close to the physical one.

The ρ meson mass for the larger lattice volume 16^4 are shown at 17 for the same set of lattice spacings. Inspecting these two figures, we do not see the strong volume dependence of the m_ρ from the magnetic field.

In addition and for the clarity we present at 18 the extrapolated value of ρ meson mass versus the squared magnetic field. The points are connected by splines. The lattice volume artefacts are not strong, but we are restricted by not sufficiently small lattice spacing and can not explore the masses at very big magnetic fields. As we know the radius of the lowest Landau level

$$r_L = \frac{1}{\sqrt{eB}}. \qquad (21)$$

We could suppose that lattice artefacts may appear at $r_L = a$, so the simple estimations give for the spacing $a = 0.0998$ fm the maximum value of the magnetic field $eB = 3.9\ GeV^2$, $2.9\ GeV^2$ for the $a = 0.1155$ fm and $2.0\ GeV^2$ for the 0.1338 fm lattice.

But from Figure 18 we see that lattice spacing artefacts appear even earlier, at $\sim 1.5\ GeV$ for the 0.1338 fm lattice and $\sim 2 \div 2.5\ GeV$ for the other lattices. Notice that for the same fields and lattice volumes the masses for the finner lattices spacing lie a litle bit higher on the plot than the masses for the coarser lattices. So we can say that the neutral ρ meson mass doesn't become zero for the fields $eB \lesssim 2\ GeV^2$ and smoothly decreases. The larger fields demands bigger and finner lattices.

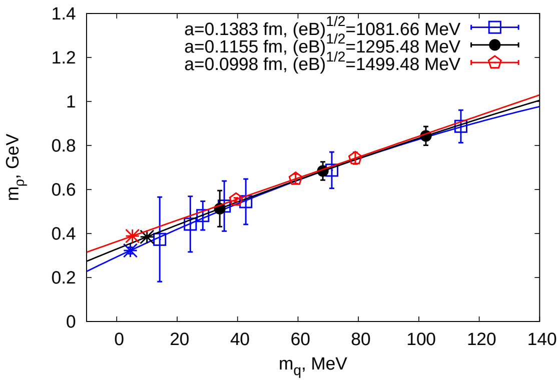

FIG. 16: The $m_{\rho_{33}}$ in depence of bare lattice quark mass for different lattice spacings, magnetic fields and 14^4 lattice volume. The extrapolated values of masses are depicted by stars and correspond to the physical quark mass $m_q^{ph} = 3$ MeV.

VIII. CONCLUSIONS

In this work we explore the masses of π, ρ and A mesons in the background of strong magnetic field of the hadronic scale. We observe that the masses extracted from different Lorentz components distinguish. The mass components extracted from the correlators of currents in the third direction along the field decrease with the value of the magnetic field, while the masses calculated from

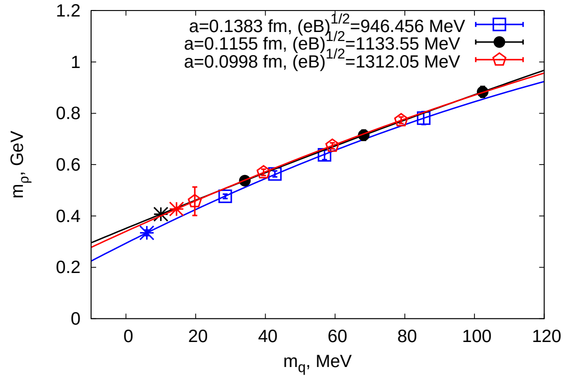

FIG. 17: The same that at Figure 16, but for 16^4 lattice volume.

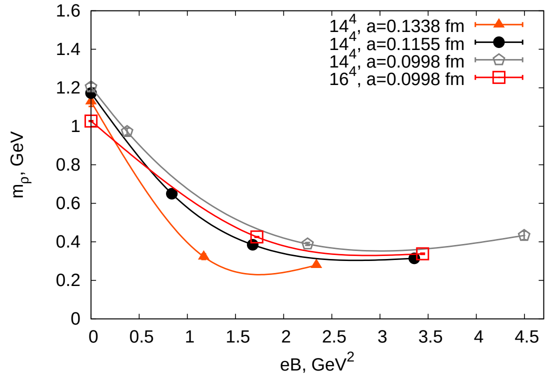

FIG. 18: The $m_{\rho_{33}}$ versus magnetic field for 14^4 lattice volume and $a = 0.1155$ fm lattice spacing. The values of masses are extrapolated to the physical quark mass $m_q^{ph} = 3$ MeV.

the currents in the directions perpendicular to the external magnetic field slowly increase for ρ meson and stay almost constant for the axial meson. Indeed the symmetry in the perpendicular directions leads to the $a_{11} \simeq a_{22}$ and $\rho_{11} \simeq \rho_{22}$. We consider this phenomena to be the result of the anisotropy, which the strong magnetic field creates. We notice that our correlators give the masses of the neutral (not charged) ρ mesons and the neutral axial mesons. The phenomena of superconductivity corresponds to the condensation of charged ρ - mesons [28]. But the superconductivity of the charged mesons, which takes place at high values of field B, also have to induce the phenomena of superfluidity, this effects was considered in QCD. The decreasing of ρ meson mass corresponds to the approaching of the superfluidity, but it seems the choice of the correlators doesn't allow to see clean so subtle effects, because of the following reasons. At first the averaging over the time slices strongly suppresses the superconductivity and superfluidity signals in our correlators, because of an inhomogeneity of the ground state perpendicular to the magnetic field. With the growth of the field value these states become more wavy and the corresponding averaging should kill such states faster. However for the not very big fields such suppression by averaging can be irrelevant and we see the decreasing of the mass along the magnetic field. So, we conclude that the observed behaviour can be an evidence of the presence of superconducting and superfluid phases at the high values of the magnetic field B [30].

IX. ACKNOWLEDGMENTS

This work was partially supported by the by the grant for Leading Scientific Schools NSh-6260.2010.2, Russian Ministry of Science and Education, contract N 07.514.12.4028, RFBR N 09-02-00629-, RFBR 11-02-01227- and 09-02-00338-a, computing facilities of the MSU Supercomputer Center have been used for our calculations. The authors are grateful to P.V. Buividovich, M.I. Polikarpov, M. Ulybyshev, V.G Zborovskii, V.G. Bornyakov, E. Akhmedov, A.S. Gorsky, M.I. Vysotsky and W. Bietenholz (Instituto de Ciencias Nucleares, UNAM) for interesting discussions and suggestions and M. N. Chernodub for very usefull comments.

[1] D. Grasso and H.R. Rubinstein, Phys. Rept. **348**, 163 (2001), arXiv:astro-ph/0009061.
[2] S.A. Voloshin, Phys. Rev. **C70**, 057901 (2004), arXiv:hep-ph/0406311.
[3] S.A. Voloshin [STAR Collaboration], arXiv:0806.0029 [nucl-ex]; H. Caines [STAR Collaboration], arXiv:0906.0305 [nucl-ex].
[4] D.E. Kharzeev, L.D. McLerran, and H.J. Warringa, Nucl. Phys. **A803**, 227 (2008), arXiv:0711.0950; K. Fukushima, D.E. Kharzeev, and H.J. Warringa, Phys. Rev. **D78**, 074033 (2008), arXiv:0808.3382; H.J. Warringa, arXiv:0906.2803; D.E. Kharzeev, arXiv:0906.2808 and arXiv:0908.0314.
[5] V. Skokov, A. Illarionov and V. Toneev, Int. J. Mod. Phys. **A24**, 5925 (2009), arXiv: 0907.1396[nucl-th].
[6] E. S. Fraga and A. J. Mizher, Phys. Rev. **D78**, 025016 (2008), arXiv:0804.1452; Nucl. Phys. **A820**, 103C (2009), arXiv:0810.3693; A.J. Mizher, M.N. Chernodub, and E.S. Fraga, Phys. Rev. **D82**, 105016 (2010), arXiv:1004.2712.
[7] R. Gatto and M. Ruggieri, Phys. Rev. **D83**, 034016 (2011), arXiv:1012.1291; R. Gatto and M. Ruggieri, Phys. Rev. **D82**, 054027 (2010), arXiv:1007.0790;
[8] K. Kashiwa, Phys. Rev. **D83**, 117901 (2010), arXiv:1104.5167.
[9] Shinya Kanemura, Haru-Tada Sato, Hiroshi Tochimura,

Nucl. Phys. **B517**, 567-598 (1998), arXiv:hep-ph/9707285.

[10] K.G. Klimenko, Theor. Math. Phys. **90**, 1-6 (1992).

[11] Massimo D'Elia, Swagato Mukherjee, Francesco Sanfilippo, Phys. Rev. **D82**: 051501 (2010), arXiv:1005.5365v2 [hep-lat].

[12] G.S. Bali, F. Bruckman, G. Endrodi, Z. Fodor, S.D. Katz, S. Krieg, A. Schafer, K.K. Szabo, JHEP, **02**, 044 (2012), arXiv:1111.4956 [hep-lat].

[13] N. O. Agasian and S. M. Fedorov, Phys. Lett. **B663**, 445 (2008), arXiv:0803.3156 [hep-ph].

[14] Paolo Cea, Leonardo Cosmai, JHEP, **0302**, 031 (2003), arXiv: hep-lat/0204023v1.

[15] Paolo Cea, Leonardo Cosmai, JHEP, **0508**, 079 (2005), arXiv: hep-lat/0505007v1.

[16] Paolo Cea, Leonardo Cosmai, Massimo D'Elia, JHEP, **0712**, 097 (2007), arXiv: 0707.1149v1 [hep-lat].

[17] V.P. Gusynin, V.A. Miransky and I.A. Shovkovy, Nucl. Phys. **B462**, 249-290 (1996), hep-ph/9509320.

[18] S. P. Klevansky and R. H. Lemmer, Phys. Rev. D **39**, 3478 (1989);

[19] D. Ebert, K. G. Klimenko, M. A. Vdovichenko and A. S. Vshivtsev, Phys. Rev. **D61**, 025005 (1999), hep-ph/9905253.

[20] E. S. Fraga and A. J. Mizher, Phys. Rev. D **78**, 025016 (2008), arXiv:0804.1452; Nucl. Phys. **A820**, 103C (2009), arXiv:0810.3693.

[21] A. Goyal, M. Dahiya, Phys. Rev. **D62**, 025022 (2000), hep-ph/9906367.

[22] N. O. Agasian and I. A. Shushpanov, Phys. Lett. **B472**, 143 (2000).

[23] T.D. Cohen, D.A. McGady, E.S. Werbos, Phys. Rev. **C76**, 055201 (2007).

[24] I. A. Shushpanov and A. V. Smilga, Phys. Lett. **B402**, 351 (1997).

[25] V.V. Braguta, P.V. Buividovich, T. Kalaydzhyan, S.V. Kuznetsov, M.I. Polikarpov, PoS LATTICE2010: **190** (2010), arXiv:1011.3795 [hep-lat].

[26] A. V. Zayakin, JHEP **0807**, 116 (2008), arXiv:0807.2917.

[27] Massimo D'Elia, Francesco Negro, Phys. Rev. **D83**: 114028 (2011), arXiv: 1103.2080v2 [hep-lat].

[28] M.N. Chernodub, Phys. Rev. Lett. **106**: 142003 (2011), arXiv:1101.0117v2 [hep-ph].

[29] V.V. Braguta, P.V. Buividovich, M.N. Chernodub, M.I. Polikarpov, arXiv:1104.3767 [hep-lat]

[30] M.N. Chernodub, Phys. Rev. **D82**, 085011 (2010) [arXiv: 1008.1055 [hep-ph]].

[31] V.G. Bornyakov, E.-M. Ilgenfritz, and M. Müller-Preussker, Phys. Rev. **D72**, 054511 (2005), hep-lat/0507021.

[32] H. Neuberger, Phys. Lett. **B417**, 141 (1998), arXiv:hep-lat/9707022.

[33] M.H. Al-Hashimi and U.J. Wiese, Annals Phys. **324**, 343 (2009), arXiv:0807.0630 [quant-ph].

[34] A.I. Vainshtein, V.I. Zakharov, V.A. Novikov and M.A. Shifman, Sov. Phys. Usp. **25**, 195 (1982) [Usp. Fiz. Nauk **136**, 553 (1982)].

[35] M. Asakawa, T. Hatsuda and Y. Nakahara, Prog. Part. Nucl. Phys. **46**, 459 (2001).

[36] R.K. Bryan, Eur. Biophys. **J18**, 165 (1990).

[37] Gert Aarts, Chris Allton, Justin Foley, Simon Hands, Phys. Rev. Lett. **99**: 022002 (2007), arXiv:hep-lat/0703008v2.

[38] F. Karsch et al, Phys. Lett. **B497**, 249 (2001).